Revision1

Equation of state of the high-pressure Fe_3O_4 phase and a new structural transition at 70 GPa

Angele Ricolleau[1,2], Yingwei Fei[2]

[1] Aix-Marseille Université, CNRS, Centre Interdisciplinaire de Nanoscience de Marseille, UMR 7325, 13288 Marseille, France

[2] Geophysical Laboratory, Carnegie Institution of Washington, 5251 Broad Branch Road, Washington, DC, 20015

Abstract

We have investigated the high-pressure behavior of Fe_3O_4 by in situ X-ray diffraction measurements from 11 to 103 GPa. Up to 70 GPa, the previous observed high-pressure Fe_3O_4 phase (h-Fe_3O_4) is stable, with a $CaTi_2O_4$-type structure. The compression curve shows an abnormal volume contraction at about 50 GPa, likely associated with the magnetic moment collapse observed at that pressure. Fitting the compression data up to 45 GPa to the Birch-Murnaghan equation of state yields a bulk modulus, K_{T0}= 172 GPa, and V_0 = 277 Å^3, with fixed K' = 4. At a pressure between 64 and 73 GPa, a new structural transition was observed in Fe_3O_4, which can be attributed to a martensitic transformation as described by Yamanaka et al. (2008) for post-spinel structural transition. The diffraction data can be best fitted with a Pnma space group. No breakdown of Fe_3O_4 was observed up to at least 103 GPa. The new high-pressure polymorph is about 6% denser than the h-Fe_3O_4 phase at 75 GPa.

Introduction

Iron exists in several oxidation states with ferrous (Fe^{2+}) and ferric (Fe^{3+}) iron being the most common in the rock-forming minerals. Magnetite Fe_3O_4 has very interesting characteristics because of the equal presence of Fe^{2+} and Fe^{3+} in its structure (Fleet, 1981). The behavior of Fe_3O_4 at high pressure and temperature is fundamentally important for understanding the oxidation state in the Earth's interior. A structural transition in magnetite was observed at around 25 GPa (Mao et al., 1974) and its high-pressure phase was first assumed to have a monoclinic structure. Fei et al. (1999) obtained X-ray diffraction data on the high-pressure phase using an imaging plate detector and monochromatic synchrotron X-radiation and proposed an orthorhombic cell with a Pbcm space group. Further structure analysis of the high-pressure phase (h-Fe_3O_4) by Haavik et al. (2000) indicated that the Cmcm space group ($CaTi_2O_4$-type structure) would better fit the observed X-ray diffraction data. Schollenbruch et al. (2011) studied the precise transition between magnetite and h-Fe_3O_4 and observed the transition at 10 GPa and 1000 K.

The stability of h-Fe_3O_4 at high pressure has been debated. Because the predicted densities of the FeO + Fe_2O_3 assemblage would become higher than that of h-Fe_3O_4 at high pressure, it has been suggested that h-Fe_3O_4 could decompose into FeO and Fe_2O_3 at sufficiently high pressure (Haavik et al., 2000). Lazor et al. (2004) predicted a breakdown of the h-Fe_3O_4 at pressures higher than 50 GPa based on thermodynamical calculations. By combining experimental data and ab initio calculation, Dubrovinsky et al. (2003) predicted that the h-Fe_3O_4 phase would be stable up to 100 GPa.

The pressure effect on iron bearing oxides is further complicated because of possible spin transitions at high pressure (Badro et al., 1999). Depending of its concentration in the

oxide and valence state, the spin transitions from high spin to intermediate or to low spin state can occur at different pressures (Badro et al., 2005). With ab initio calculation, Ju et al. (2012) predicted a phase transition in magnetite from cubic to orthorhombic Pbcm space group at 30 GPa as previously observed and a second transition at 65 GPa to an orthorhombic Cmcm space group. They showed that the two transitions were caused by spin transitions in iron from high spin to intermediate spin at 30 GPa and then to low spin at 65 GPa. The second transition at 65 GPa is associated with an abrupt decrease in the magnetic moment of iron in one site of orthorhombic structure changing from intermediate to low spin state. Another ab initio study concluded that Fe_3O_4 had no spin transition in iron up to 45 GPa (Bengston et al., 2013). An experimental study from Xu et al. (2004) showed an incipient metallic behavior in Fe_3O_4 coupled with a magnetic moment collapse above 50 GPa, Fe_3O_4 becoming nonmagnetic after 70 GPa.

In this study, we obtained X-ray diffraction (XRD) patterns on Fe_3O_4 at pressures from 11 GPa to 103 GPa. We observed the formation of h-Fe_3O_4 and determined its equation of state up to 70 GPa. After 70 GPa, we observed a structural transition to another orthorhombic structure with Pnma space group.

EXPERIMENTAL METHODS

We used Fe_3O_4 magnetite from Alfa Aesar (99.95% purity) as the starting material. Approximately 7 wt% of high purity gold powder was mixed with magnetite powder and gold served as the pressure calibrant. One diamond anvil cells (DAC) was loaded with the mixture in argon pressure transmitting medium (run #1) and a second DAC, in neon pressure medium (run #2). After performing the first two experiments in which a structure transition was observed, we loaded a third DAC with the mixture in neon medium to collected additional

diffraction data around the transition pressure. Anvils with 300 μm culets and beveled anvils with 200 μm culets were used. Re gasket were pre-indented to a thickness of 25-30 μm and then drilled sample holes with diameters of 130 μm to 200 μm depending on the culet size.

In situ XRD measurements were carried out at the GSECARS (13IDD) sector of the Advanced Photon Source (Argonne National Laboratory) with a fixed wavelength of 0.3344 Å. High temperature was achieved by double-sided laser-heating (Shen et al. 2001; Prakapenka et al. 2008). The 20 μm laser heating spot with relatively uniform temperature was carefully aligned with a 6-μm X-ray spot to obtain diffraction data at simultaneous high pressure and temperature. Temperature measurements were acquired from both sides during each XRD acquisition. In general, we first compressed the sample to a targeted pressure at room temperature and then laser-heated sample to high temperatures. *In situ* XRD patterns were collected from 11 GPa to 103 GPa, at room temperature and high temperature up to 2300 K. Only room-temperature data obtained after annealing were presented in this study.

Pressures were calculated from the equation of state of gold (Fei et al., 2007a). Quasi-hydrostatic environment was achieved with neon pressure medium (Meng et al., 1993). We obtained 17 XRD patterns at room temperature, integrated from two-dimensional diffraction patterns with the Fit2d program (Hammersley et al., 1996). Rietveld refinements of the *in situ* XRD patterns were performed to determine the volumes of present phases with the GSAS software package (Larson and Von Dreele, 1994) and the EXPGUI interface (Toby, 2001). After convergence, the values of R_{wp} were always lower than 0.03. The crystal structure of the phases, atomic positions, and thermal parameters from the literature were used as the fixed parameters to refine the unit cell parameters.

RESULTS AND DISCUSSION

We have conducted three experiments and obtained XRD spectra of Fe_3O_4 up to 103 GPa. During the first experiment, we collected diffraction data from 11 to 26 GPa (run #1). Both magnetite and h-Fe_3O_4 were present in these patterns. For the second experiment, we directly compressed Fe_3O_4 to 45 GPa, and then heated the sample to high temperatures using the double-sided laser-heating system at the beamline. The sample pressures were gradually increased to 103 GPa (run #2). At each pressure, we carried out heating cycles to anneal the sample and monitor the change of the XRD patterns. We observed the presence of h-Fe_3O_4 only from 45 to 64 GPa. During the heating cycles, we did not observe any new diffraction peaks besides those of h-Fe_3O_4, indicating no structure change upon heating. At pressures higher than 64 GPa, several new diffraction peaks appeared, caused by a transition from h-Fe_3O_4 to a new high-pressure phase. We attempt to constrain this transition with a third experiment (run #3), where Fe_3O_4 sample was directly compressed at 64 GPa and then at 76 GPa, using the same experimental procedure. We used neon as the pressure calibrant (Fei et al., 2007a) for run #3 because gold diffraction peaks were not observed.

Equation of state of high-pressure Fe_3O_4

First, we check the structure of the high-pressure phase of magnetite in our patterns because the space group assignment is still debated. Fei et al. (1999) first suggested a Pbcm space group. Haavik et al. (2000) indicated that the powder diffraction data are more consistent with a Cmcm space group assignment, whereas ab initio calculation of Ju et al. (2012) showed that a structure with a Pbcm space group is stable. We tested the $CaTi_2O_4$-type structure (Cmcm) with the atomic position from Haavik et al. (2000) and a $CaMn_2O_4$-type structure (Pbcm) with atomic position from Fei et al. (1999). The $CaTi_2O_4$-type structure give a very subtle better fit compare to the $CaMn_2O_4$-type as also observed by Haavik et al. (2000). We also evaluated the atomic positions of the Cmcm structure type given by Dubrovinsky et al. (2003) for h-Fe_3O_4 and by Yamanaka et al. (2009) for Fe_2TiO_4. The fitting results are very

similar, which do not permit us to distinct between these atomic positions. Because Pnma is a subgroup of Cmcm and of Pbcm (Hahn, 1983), we also evaluated if the Pnma space group would yield a better fit. For Pnma space group, we used atomic positions of Cmcm structure given by Haavik et al. (2000) and transformed it to a Pnma space group (Stokes and Hatch, 1988). The refinements by using the three space groups produced similar fitting results to the observed XRD patterns. The fitting parameters are listed in Table 1 for the XRD pattern obtained at 64 GPa in run #2 with no gold. Because Pnma is the lower symmetry space group, it is expected that the error for Pnma is slightly smaller than that for Pbcm after refining the atomic positions. Although the refinement with a Pbcm showed a slightly smaller error than the Cmcm refinement, the favored space group assignment is Cmcm because of its higher symmetry space group. The same conclusion has been made by Sun et al. (2009) on AlH_3 where they showed that space groups R3c, Pbcm and Pnma gave the same satisfactory Rietveld refinement results and the structure with the highest symmetry space group was favored.

We choose to fit our XRD patterns by a Rietveld analysis method using the Cmcm structure (i.e., the higher symmetry space group) with the atomic positions from Haavik et al. (2000) for consistency since not all of our XRD patterns permit us to refine the atomic positions. The refined unit cell parameters for h-Fe_3O_4 are listed in Table 2. Figure 1 shows the volume of magnetite and h-Fe_3O_4 up to 70 GPa obtained in this study compared to the literature data. At pressures between 11 GPa and 26 GPa, magnetite coexists with the high-pressure phase. Our refined volumes of magnetite are in a good agreement with those obtained by Haavik et al. (2000), whereas volumes of h-Fe_3O_4 show smaller values (Fig. 1). We also compared our volumes with data from Dubrovinsky et al. (2003), Mao et al. (1974), Lazor et al. (2004), and Fei et al. (1999). Our results are consistent with those of Lazor et al. (2004), Mao et al. (1974), and Fei et al. (1999). The data point of Haavik et al. (2000) at 40

GPa refined with Cmcm structure is also consistent with our results. The difference in the refined volumes between this study and Haavik et al. (2000) could come from fitting procedure. For example, the volumes of h-Fe_3O_4 given in their Table 4 were obtained by using the $CaMn_2O_4$-type structure (Pbcm) with V= 239.8(1.6) $Å^3$ at 40 GPa, whereas the refined volume is V= 235.3(0.5) $Å^3$ with the Cmcm space group (see their Table 5) at the same pressure which plots on our compression curve (Fig. 1). In addition, we heat the sample up to about 2100 K and acquired patterns after heating, whereas Haavik et al. (2000) did not heat their sample. There might be some structural distinctions between h-Fe_3O_4 transformed at 300 K and the annealed h-Fe_3O_4. Hazen and Navrotsky (1996) discussed the importance of the volume of disordering in spinels with pressure. They mentioned a difference between disordered volume and ordered volume up to 5% in oxides with cations involving mixed valence and coordination. The h-Fe_3O_4 volume difference between those of Haavik et al. (2000) and ours is about 2% and could be explained by cation ordering with annealing.

Lazor et al. (2004) predict that h-Fe_3O_4 becomes unstable above 50 GPa, favoring the breakdown to Fe_2O_3 and FeO. We have obtained diffraction data up to 103 GPa and did not observe any breakdown. Figure 2 shows representative X-ray diffraction patterns at different pressures. The patterns up to 64 GPa showed no new peaks other than the ones that belong to h-Fe_3O_4 (Fig. 2). Upon heating the observed XRD patterns remain the same with just systematic peak position shifts, indicating no oxidation change or breakdown reaction to form Fe_2O_3 or FeO. New diffraction peaks did appear at pressures above 73 GPa which are caused by a structure transition in Fe_3O_4 as discussed below.

We fitted the compression data of h-Fe_3O_4 to the Birch-Murnaghan equation and obtained a bulk modulus K_0 of 124 ±12 GPa and an initial volume V_0 of 287±4 $Å^3$ with the derivative of the bulk modulus K' fixed to 4 by fitting the entire dataset up to 64 GPa. As shown in Figure 1, the calculated compression curve using these parameters does not

reproduce the measured volumes well, particularly in the pressure range of 11 and 45 GPa. By examining the axial compression behavior, we found an abrupt contraction of *a*-axis at a pressure between 45 and 50 GPa (Table 2). The insert in Figure 1 shows the a/c ratio change as a function of pressure, indicating a clear discontinuity at about 50 GPa. The fit of the compression data up to 45 GPa yielded K_0= 172±8 GPa and V_0= 277±2 $Å^3$. The derived bulk modulus is smaller than values reported in previous studies (Table 3). It is also smaller than the value of magnetite (K_0= 186 GPa) (Reichmann and Jacobsen, 2004).

Phase transition in high pressure magnetite

At pressures above 70 GPa, we observed the appearance of new diffraction peaks in the XRD patterns (Figure 2). Lazor et al. (2004) predicted the disproportion of Fe_3O_4 to FeO and Fe_2O_3 above 50 GPa. We checked for a potential presence of FeO and ruled out this possibility based on the observed diffraction peaks which do not match the FeO diffraction peaks at these pressures. Testing the presence of hematite is more complicated since the high-pressure form of hematite is still uncertain (Ito et al., 2009; Shim et al., 2009). However, we collected many diffraction patterns around the transition pressure at different temperatures and observed consistent patterns of h-Fe_3O_4 and the new post h-Fe_3O_4 phase. We conclude that no breakdown has taken place in Fe_3O_4. The changes observed in the patterns must be caused by a second structural transition in Fe_3O_4.

An ab initio study (Ju et al., 2012) proposed a structural transition in h-Fe_3O_4 at 65 GPa, which is in agreement with our observation. However, their proposed structure with a Cmcm space group does not fit the observed new diffraction patterns for the post h-Fe_3O_4 phase. We have researched possible structures of the post-spinel phases, particularly the high-pressure structures obtained on different high-pressure post-spinel phases such as $CaMn_2O_4$, $CaFe_2O_4$ (Yamanaka et al., 2008) and Fe_2TiO_4 (Yamanaka et al., 2013). Yamanaka et al.

(2013) observed a transition in Fe_2TiO_4 at around 60 GPa. They proposed a Pmma space group for the new high-pressure post-spinel phase in Fe_2TiO_4. We used this orthorhombic structure to index the observed diffraction peaks, but failed to obtain a satisfactory solution. We have further tested the post-spinel structure of $CaTi_2O_4$ and $CaFe_2O_4$ given by Yamanaka et al. (2008), in which they observed a shift in atomic positions with pressure giving orthorhombic cells with displacing atoms in every third layer perpendicular to the *c* axis. This gives a three times bigger orthorhombic cell compared to the usual ones. Because h-Fe_3O_4 can be fitted with a Cmcm space group, we tried the high-pressure form of $CaTi_2O_4$ post-spinel which corresponds to a Cmcm orthorhombic cell that is three times larger than the h-Fe_3O_4 unit cell. The Le bail method refinement gave a better fit compared to the one using the Pmma space group, but all diffraction peaks cannot be fitted with this structure.

Finally, we tested the high-pressure form of $CaFe_2O_4$ type structure (Yamanaka et al., 2008) which also corresponds to a three times larger cell of an orthorhombic form, but with a Pnma space group. The Le Bail refinement gives the best satisfactory result that indexes all the observed diffraction peaks. We conclude that the new post h-Fe_3O_4 phase at 70 GPa could have a Pnma space group with a spinel regular cell multiplied by 3. However, there is not enough information to constrain the atomic positions.

In the post h-Fe_3O_4 phase at pressures above 70 GPa, there are so many observed peaks and the LeBail refinement is not constrained enough and could give several volume values. To be more accurate in the volume determination, we used a Rietveld refinement with the atomic positions of Haavik et al. (2000) for a Cmcm space group transformed to a Pnma space group with an initial cell size multiplied by 3. Although it gives a high chi-value due to uncertainties in the estimated intensities, it permits us to obtain a better volume estimate of the new structure. Using this structure model, we then fitted the diffraction patterns by Le Bail

method. Figure 3 shows a representative refinement result at 76.5 GPa. The refined volumes and unit cell parameters are listed in Table 2.

We have examined the phase transition boundary by two laser-heating cycles started at 64 and 73 GPa at room temperature respectively. Figure 4 plots the stability of h-Fe_3O_4 and the new post h-Fe_3O_4 phase at high temperature and pressure. During the heating cycle at 64 GPa up to 2050 K, we observed only h-Fe_3O_4. After quenching to room temperature, we increased pressure to 73 GPa where the new post h-Fe_3O_4 phase appeared. During the heating cycle at 73 GPa up to 2050 K, only the post h-Fe_3O_4 phase was observed. The inferred Clapeyron slope of the phase boundary may be slightly positive.

Fe_3O_4 shows complex behavior in its electronic and magnetic properties at high pressure. Ding et al. (2008) proposed a magnetic transition attributed to a high spin to intermediate spin transition of Fe^{2+} between 12 and 16 GPa, whereas Baudelet et al. (2010) argued for no electronic and magnetic abrupt transition up to 41 GPa. Very few experimental studies have been focused on high-pressure behavior of Fe_3O_4. Xu et al. (2004) showed three distinct ranges in the resistivity of Fe_3O_4: an increase between 20 to 40-50 GPa, a rapid decrease up to 70 GPa, and a regular decrease up to 140 GPa. They suggested a gradual Fe^{3+} moment collapse starting at 50 GPa and becoming nonmagnetic at 80 GPa. The observed abrupt change in *a*-axis in this study (Fig. 1 insert) could be associated with observed change in resistivity of Fe_3O_4 at 50 GPa (Xu et al., 2004). The change in compression and resistivity behavior after 50 GPa could be followed by a spin transition in iron, as observed in many iron oxides at high pressure (e.g., Badro et al., 1999; Fei et al., 2007b; Badro et al., 2002; Shim et al., 2009; Merlini et al., 2010; Lavina et al., 2010).

Figure 5 plots our compression data up to 103 GPa, together with the calculated compression curves, compared with results on different spinels. The comparison may provide

insights to Fe^{2+} and Fe^{3+} spin transitions at high pressure. Fei et al. (2007b) show that the ion radii of the low-spin Fe^{2+} and Mg^{2+} are similar. By studying the compression behavior of (Mg, Fe)O with increasing pressure, they showed that the compression curves of (Mg, Fe)O merge with that of MgO once Fe^{2+} is in the low spin state. The volumes of h-Fe_3O_4 at 52 GPa and 64 GPa are plotted on the compression curve of post-spinel $MgFe_2O_4$ reported by Andrault and Bolfan-Casanova (2001). This is consistent with Fe^{2+} in h-Fe_3O_4 being at low-spin state, supporting the hypothesis that Fe^{2+} in h-Fe_3O_4 undergoes a spin transition at about 50 GPa.

We also compare our data with $CaFe_2O_4$ compression curves for iron in high and low spin states (Merlini et al., 2010) in which the spin transition takes place around 50 GPa. The volume difference between their two compression curves is about 6%. The transition from h-Fe_3O_4 to the post h-Fe_3O_4 phase results in comparable volume reduction, which may be associated with the spin transition of Fe^{3+}. An ab initio study (Ju et al., 2012) showed gradual spin transitions of ions in Fe_3O_4 from high spin to intermediate spin of iron at about 65 GPa. Spin transition of Fe^{3+} in high-pressure iron oxides have been observed, such as, in Fe_2O_3 and in $CaFe_2O_4$ (Badro et al., 2002; Merlini et al., 2010). It is often associated with a magnetism collapsing, observed at high pressure in Fe_2O_3 (Pasternak et al., 1999) and in Fe_3O_4 (Xu et al., 2004). The observed volume reduction in h-Fe_3O_4 and the structure transition to the post h-Fe_3O_4 phase are likely associated with the spin transitions of Fe^{2+} and subsequently Fe^{3+} in the high-pressure phases. Additional spectroscopic studies at high pressure are needed to gain insights to the iron spin transitions in Fe_3O_4.

IMPLICATIONS

We have confirmed the high-pressure Fe_3O_4 phase (h-Fe_3O_4) has an orthorhombic structure. The most probable space group for h-Fe_3O_4 is Cmcm. A least-squares fit of the compression data of h-Fe_3O_4 up to 45 GPa yields the EOS parameters of K_0= 172±8 GPa and V_0= 277±2 Å^3, with fixed K' = 4. We observed a volume contraction without structure change at about 50 GPa, which is likely caused by a spin transition of Fe^{2+} in h-Fe_3O_4. This suggestion is also supported by the observed changes in the magnetic behavior of Fe_3O_4 at 50 GPa (Xu et al., 2004) and the DFT calculations (Siberchicot, 2013; Ju et al., 2012). In addition, we observed a new structural transition in Fe_3O_4 at a pressure between 64 and 73 GPa. This new post h-Fe_3O_4 phase has an orthorhombic structure with a likely Pnma space group and the Clapeyron slope of the phase boundary between h-Fe_3O_4 and the post h-Fe_3O_4 phase is positive.

Knowledge of compression behavior, spin state of iron ions, and structure transitions of iron oxides at high pressure and temperature is essential for understanding the role of iron in the Earth's mantle. The bulk iron content in the Earth's mantle is about 8 wt%, distributed between ferropericlase and mantle silicates in the forms of Fe^{2+} and Fe^{3+}. Iron spin transitions in ferropericlase and Fe-bearing bridgmanite have been extensively studied (e.g., Badro et al., 2005; Fei et al., 2007b; Li et al. 2004; Lin et al. 2013; Jackson et al., 2005). The observed transitions in Fe_3O_4 provide further understanding of spin transitions of Fe^{2+} and Fe^{3+} at high pressure and their effect on the density and element partitioning in lower mantle minerals.

Fe_3O_4 contains both Fe^{2+} and Fe^{3+} with different spin states at high pressure. As demonstrated, the electronic and structural transitions could significantly change the compression behavior of Fe_3O_4. As an important component in the iron oxide buffer system, accurate equation of state of Fe_3O_4 over a large pressure and temperature range is essential for calibrating the buffers involving Fe_3O_4 under mantle conditions. Campbell et al. (2009) showed the effect of pressure on the iron-wüstite oxygen fugacity buffer at high pressure.

With the measured equations of state of different Fe_3O_4 phases, we can now calculate the FeO-Fe_3O_4 buffer as a function of pressure. The new structural transition shows a volume drop of about 6 % relative to the compression curve of h-Fe_3O_4. This volume change could have a strong impact on the buffer involving Fe_3O_4. Further experiments are required to better constrain the space group and atomic positions, and its equation of state.

Acknowledgements

This work was supported by NSF geophysics grant to YF and by the Carnegie Institution of Washington. We thank V. Prakapenka and P. Dera for technical assistance and C. Seagle for collecting part of the experimental data. The X-ray diffraction data were collected at APS GSECARS beamline supported by NSF, DOE, and the State of Illinois.

References

Andrault, D., and Bolfan-Casanova, N. (2001) High-pressure phase transformations in the $MgFe_2O_4$ and Fe_2O_3-$MgSiO_3$ systems. Physics and Chemistry of Minerals, 28, 211-217.

Badro, J., Struzhkin, V.V., Shu, J., Hemley, R.J., and Mao, H-K. (1999) Magnetism in FeO at megabar pressures from X-ray emission spectroscopy. Physical Review Letters, 83, 20, 4101-4104.

Badro, J., Fiquet, G., Struzhkin, V.V., Somayazulu, M., Mao, H-K., Shen, G., and Le Bihan, T. (2002) Nature of the High-pressure transition in Fe_2O_3 hematite. Physical Review Letters, 89, 20, doi: 10.1103/PhysRevLett.89.205504.

Badro, J., Fiquet, G., and Guyot, F. (2005) Thermochemical state of the lower mantle: new insights from mineral physics. Earth's Deep Mantle: Structure, Composition, and Evolution, Geophysical Monograph Series 160, p 241-260.

Baudelet, F., Pascarelli, S., Mathon, O., Itié, J-P., Polian, A., and Chervin, J-C. (2010) Absence of abrupt pressure-induced magnetic transitions in magnetite. Physical Review B, 82, 140412.

Bengston, A., Morgan, D., and Becker, U. (2013) Spin state of iron in Fe_3O_4 magnetite and h-Fe_3O_4. Physical review B, 87, 155141.

Campbell, A.J., Danielson, L., Righter, K., Seagle, C.T., Wang, Y., and Prakapenka, V.B. (2009) High pressure effects on the iron-iron oxide and nickel-nickel oxide oxygen fugacity buffers. Earth and Planetary Science Letters, 286, 556-564.

Ding, Y., Haskel, D., Ovchinnikov, S.G., Tseng, Y-T., Orlov, Y.S., Lang, J.C., and Mao, H-K. (2008) Novel pressure-induced magnetic transition in magnetite (Fe3O4). Physical Review Letters, 100, 045508.

Dubrovinsky, L.S., Dubrovinskaia, N.A., McCammon, C., Rozenberg, G.Kh., Ahuja, R., Osorio-Guillen, J.M., Dmitriev, V., Weber, H.P., LeBihan, T., and Johanson, B. (2003) The structure of the metallic high-pressure Fe_3O_4 polymorph: experimental and theoretical study. Journal of Physic: Condensed Matter, 15, 7697-7706.

Fei, Y., Frost, D.J., Mao, H-K., Prewitt, C., and Hausermann, D. (1999) In situ structure determination of the high-pressure phase of Fe_3O_4. American Mineralogist, 84, 203-206.

Fei, Y., Ricolleau, A., Frank, M., Mibe, K., Shen, G., and Prakapenka, V. (2007a) Toward an internally consistent pressure scale. Proceeding of the National Academy of Sciences of the United States of America, doi:10.1073/pnas.0609013104.

Fei, Y., Zhang, L., Corgne, A., Watson, H., Ricolleau, A., Meng, Y., and Prakapenka, V. (2007b) Spin transition and equations of state of (Mg, Fe)O solid solutions. Geophysical Research Letters, 34, L17307, doi:10.1029/2007GL030712.

Fleet, M.E. (1981) The structure of magnetite. Acta Crystallographica section B-Structural science, 37, 917-920, doi:10.1107/S0567740881004597.

Haavik, C., Stolen, S., Fjellvag, H., Hanfland, M., and Häusermann, D. (2000) Equation of state of magnetite and its high-pressure modification: Thermodynamics of the Fe-O system at high pressure. American Mineralogist, 85, 514-523.

Hahn, T.D. (1983) International Tables for Crystallography, volume A: Space Group Symmetry. Reidel Publishing Company, Dordrecht.

Hammersley, A.P., Svensson, S.O., Hanfland, M., Fitch, A.N., and Hausermann, D. (1996) Two-dimmensional detector software: From real detector to idealized image or two-theta scan. High pressure Research, 14, 235-245, doi:10.1016/S0012-821X(03)00361-3.

Hazen, R.M., and Navrotsky, A. (1996) Effects of pressure on order-disorder reactions. American Mineralogist, 81, 1021-1035.

Ito, E., Fukui, H., Katsura, T., Yamazaki, D., Yoshino, T., Aizawa, Y., Kubo, A., Yokoshi, S., Kawabe, K., Zhai, S., Shatzkiy, A., Okube, M., Nozawa, A., and Funakoshi, K-I. (2009) Determination of high-pressure phase equilibria of Fe_2O_3 using the Kawai-type apparatus equipped with sintered diamond anvils. American Mineralogist, 94, 205-209, doi: 10.2138/am.2009.2913.

Jackson, J.M., Sturhahn, W., Shen, G., Zhao, J., Hu, M.Y., Errandonea, D., Bass, J.D., and Fei, Y. (2005) A synchrotron Mösbauer spectroscopy study of $(Mg,Fe)SiO_3$ perovskite up to 120 GPa. American Mineralogist, 90, 199-205.

Ju, S., Cai, T.Y., Lu, H.S., and Gong, C.D. (2012) Pressure-induced crystal structure and spin-state transitions in magnetite (Fe_3O_4). Journal of the American Chemical society, 134, 13780-13786, doi: 10.1021/ja305167h.

Knittle, E., and Jeanloz, R. (1986) High-pressure metallization of FeO and implications for the Earth's core. Geophysical Research Letters, 13, 1541-1544.

Larson, A. C., and R. B. Von Dreele (2000) General structure analysis system (GSAS), Los Alamos National Laboratory Report LAUR, 86-748.

Lavina, B., Dera, P., Downs, R.T., Yang, W., Sinogeikin, S., Meng, Y., Shen, G., and Schiferl, D. (2010) Structure of siderite FeCO3 to 56 GPa and hysteresis of its spin-pairing transition. Physical Review B, 82, 064110.

Lazor, P., Shebanova, O.N., and Annersten, H. (2004) High-pressure study of stability of magnetite by thermodynamic analysis and synchrotron X-ray diffraction. Journal of Geophysical Research, 109, B05201, doi:10.1029/2003JB002600.

Li, J., Struzhkin, V.V., Mao, H.K., Shu, J., Hemley, R.J., Fei, Y., Mysen, B., Dera, P., Prakapenka, V., and Shen, G. (2004) Electronic spin state of iron in lower mantle perovskite. Proceeding of the National Academy of Sciences of the United States of America, 101, 14027–14030.

Lin, J. F., Speziale, S., Mao, Z., and Marquardt, H. (2013) Effects of the electronic spin transitions of iron in lower-mantle minerals: implications to deep-mantle geophysics and geochemistry. Reviews of Geophysics, 51, 244–275.

Mao, H-K., Takahashi, T., Bassett, W.A., Kinsland, G.L., and Merrill, L. (1974) Isothermal compression of magnetite to 320 kbar and pressure-induced phase transformation. Journal of geophysical research, 79, 8, 1165-1170.

Meng, Y., Weidner, D.J., and Fei, Y. (1993) Deviatoric stress in a quasi-hydrostatic diamond anvil cell: Effect on the volume-based pressure calibration. Geophysical Research Letter, 20, 1147-1150.

Merlini, M., Hanfland, M., Gemmi, M., Huotari, S., Simonelli, L., and Strobel, P. (2010) Fe^{3+} spin transition in $CaFe_2O_4$ at high pressure. American Mineralogist, 95, 200-213.

Murakami, M., Hirose, K., Ono, S., Tshuchiya, T., Isshiki, M., and Watanuki, T. (2004) High pressure and high temperature phase transitions of FeO. Physics of the Earth and Planetary Interiors, 146, 273-282.

Ono, S., Hirose, K., Kikegawa, T., and Saito, Y. (2002) The compressibility of a natural composition calcium ferrite-type aluminous phase to 70 GPa. Physics of the Earth and Planetary Interiors, 131, 311-318.

Pasternak, M.P., Rozenberg, G.Kh., Machavariani, G.Yu., Naaman, O., Taylor, R.D., and Jeanloz, R. (1999) Breakdown of the Mott-Hubbard state in Fe_2O_3: a first-order insulator-metal transition with collapse of magnetism at 50 GPa. Physical Review Letters, 82, 4663-4666.

Prakapenka, V. B., Kubo, A., Kuznetsov, A., Laskin, A., Shkurikhin, O., Dera, P., Rivers, M.L., and Sutton, S.R. (2008) Advanced flat top laser heating system for high pressure research at GSECARS: application to the melting behavior of germanium. High Pressure Research, 28, 225-235.

Reichmann, H.J., and Jacobsen, S.D. (2004) High-pressure elasticity of a natural magnetite crystal. American Mineralogist, 89, 1061-1066.

Schollenbruch, K., Woodland, A.B., Frost, D.J., Wang, Y., Sanehira, T., and Lagenhorst, F. (2011) In situ determination of the spinel-post spinel transition in Fe_3O_4 at high pressure and high temperature by synchrotron X-ray diffraction. American Mineralogist, 96, 820-827.

Shen, G., Rivers, M.L., Wang, Y., and Sutton, S. R. (2001) A laser heated diamond cell system at the Advanced Photon Source for in situ x-ray measurements at high pressure and temperature. Review of Scientific Instruments, 72, 1273-1282.

Sherman, D.M. (1989) The nature of the pressure-induced metallization of FeO and its implications to the core-mantle boundary. Geophysical Research Letters, 16, 515-518.

Shim, S-H., Bengtson, A., Morgan, D., Sturhahn, W., Catalli, K., Zhao, J., Lerche, M., and Prakapenka, V. (2009) Electronic and magnetic structures of the postperovskite-type Fe_2O_3 and implications for planetary magnetic records and deep interiors. Proceeding of the National Academy of Sciences of the United States of America, 106, 14, 5508-5512, doi: 10.1073/pnas.0808549106.

Siberchicot, B. (2013) On the optical properties and low pressure-induced spin transition in magnetite from ab initio calculations. Journal of magnetism and magnetic materials, 335, 86-89.

Stokes, H.T., Hatch, D.M. (1988) Isotropy subgroup of the 230 crystallographic space groups. World Scientific Publishing Co. Pte. Ltd., p 9, p 1-56.

Sun, S., Ke, X., Chen, C., and Tanaka, I. (2009) First-principles prediction of low-energy structures for AlH_3. Physical Review B, 79, 024104.

Toby, B.H. (2001) EXPGUI, a graphical user interface for GSAS. Journal of Applied Crystallography, 34, 210-213.

Vanpeteghem, C.B., Angel, R.J., Ross, N.L., Jacobsen, S.D., Dobson, D.P., Litasov, K.D., and Ohtani, E. (2006) Al, Fe substitution in the $MgSiO_3$ perovskite structure: A single-crystal X-ray diffraction study. Physics of the Earth and Planetary Interiors, 155, 96-103.

Xu, W.M., Machavariani, G.Y., Rozenberg, G.K., and Pasternak, M.P. (2004) Mössbauer and resistivity studies of the magnetic and electronic properties of the high-pressure phase of Fe_3O_4. Physical Review B, 70, 174106.

Yamanaka, T., Uchida, A., and Nakamoto, Y. (2008) Structural transition of post-spinel phases $CaMn_2O_4$, $CaFe_2O_4$, and $CaTi_2O_4$ under high pressures up to 80 GPa. American Mineralogist, 93, 1874-1881.

Yamanaka, T., Mine, T., Asogawa, S., and Nakamoto, Y. (2009) Jahn-Teller transition of Fe2TiO4 observed by maximum entropy method at high pressure and low temperature. Physical Review B, 80, 134120.

Yamanaka, T., Kyono, A., Nakamoto, Y., Meng, Y., Kharlamova, S., Struzhkin, V.V., and Mao, H.K. (2013) High-pressure phase transitions of Fe_{3-x} Ti_x O_4 solid solution up to 60 GPa correlated with electronic spin transition. American Mineralogist, 98, 736-744.

Figures captions

Figure 1: volume of magnetite and h-Fe_3O_4 obtained at high pressure (using gold pressure scale) and room temperature in this study are shown together with data from the literature. Compression curves obtained using dataset up to 45 GPa (1) and 64 GPa (2) and obtained by Haavik et al. (2000) on h-Fe_3O_4 are shown for comparison. The inserted figure shows the change of a/c ratio as a function of pressure.

Figure 2: XRD patterns of magnetite with pressure showing h-Fe_3O_4 diffraction peaks and the new structure after 70 GPa. Black and grey tick marks correspond to Neon and gold diffraction peaks respectively.

Figure 3: XRD pattern measured at 76.5 GPa (Neon pressure) fitted by Le Bail method with a Pnma space group obtained from the Cmcm unit cell of Haavik et al. (2000) transformed to

Pnma and multiplied by three. Cell parameters are a = 8.851(1) Å, b = 7.8370(6) Å and c = 8.660(1) Å.

Figure 4: Presence of h-Fe_3O_4 or the new structure with pressure and temperature as observed in our XRD patterns.

Figure 5: Volume of magnetite and its high pressure forms as a function of pressure plotted with compression curves obtained in this study using data up to 45 GPa. For comparison, compression curves from several spinel has been plotted; CF type from MORB from Ono et al. (2002); $CaFe_2O_4$ LS and HS, low spin and high spin EOS parameters from Merlini et al. (2010); $MgFe_2O_4$, compression curve from Andrault and Bolfan-Casanova (2001).

Table 1: Result of h-Fe_3O_4 cell parameters and atomic positions fitted with three orthorhombic space groups with the XRD pattern at 64 GPa.

Cmcm				**Pbcm**				**Pnma**			
Rwp = 0.0052				Rwp = 0.0050				Rwp = 0.0048			
Reduced χ2 = 0.2976E-01				Reduced χ2 = 0.2829E-01				Reduced χ2 = 0.2581E-01			
a = 2.63880(33)				a = 2.63886(33)				a = 9.05338(99)			
b = 8.88490(142)				b = 8.88442(139)				b = 2.63839(31)			
c = 9.05426(99)				c = 8.88668(140)				c = 8.88668(140)			
Atomic positions				Atomic positions				Atomic positions			
	x	y	z		x	y	z		x	y	z
Fe1	0.0	0.3830(7)	0.25	Fe1	0.782(8)	0.3675(7)	0.25	Fe1	0.0592(12)	0.75	0.8794(13)
Fe2	0.0	0.1365(7)	0.0713(5)	Fe2	0.277(6)	0.1128(7)	0.0726(6)	Fe2	0.2416(21)	0.75	0.1346(7)
O1	0.0	0.0486(28)	0.25	O1	0.718(30)	0.25	0.0	Fe3	0.9124(14)	0.75	0.6062(14)
O2	0.0	0.2430(22)	0.6014(15)	O2	0.209(24)	0.2001(29)	0.25	O1	0.609(7)	0.75	0.987(8)
O3	0.0	0.5	0.0	O3	0.260(24)	0.4903(22)	0.1022(15)	O2	0.027(5)	0.75	0.277(4)
								O3	0.257(9)	0.75	0.7978(28)
								O4	0.398(6)	0.75	0.508(9)
Bond distances				Bond distances				Bond distances			
	Fe1-Fe1	2.63880(33)	x2		Fe1-Fe1	2.63886(33)	x2		Fe1-Fe1	2.63839(31)	x2
	Fe1-Fe2	2.722(7)	x2		Fe1-Fe2	2.712(7)	x2		Fe1-Fe1	2.735(20)	x2
	Fe1-O1	1.976(20)	x2		Fe1-O1	2.498(6)	x2		Fe1-Fe2	2.806(18)	
	Fe1-O2	2.192(14)	x4		Fe1-O2	2.12(5)			Fe1-Fe3	2.768(12)	
	Fe1-O3	2.4910(25)	x2		Fe1-O2	1.87(4)			Fe1-O2	2.067(26)	x2
					Fe1-O3	2.21(4)	x2		Fe1-O3	1.93(8)	
	Fe2-Fe2	2.63880(33)	x2		Fe1-O3	2.14(4)	x2		Fe1-O4	1.79(5)	x2
	Fe2-Fe2	2.749(11)							Fe1-O4	1.77(7)	
	Fe2-Fe2	2.734(11)	x2		Fe2-Fe2	2.63886(33)	x2				
	Fe2-O1	1.797(10)			Fe2-Fe2	2.809(20)			Fe2-Fe2	2.63839(31)	x2
	Fe2-O2	1.828(13)			Fe2-Fe2	2.670(18)			Fe2-Fe3	2.640(18)	
	Fe2-O2	1.721(14)	x2		Fe2-Fe2	2.769(12)			Fe2-O1	2.17(5)	x2
	Fe2-O3	1.905(4)	x2		Fe2-O1	2.02(6)			Fe2-O2	2.32(6)	
					Fe2-O1	1.81(5)			Fe2-O2	2.70(6)	
					Fe2-O2	1.793(12)			Fe2-O3	1.960(20)	x2
					Fe2-O3	1.81(5)			Fe2-O4	2.14(5)	x2
					Fe2-O3	1.66(5)					
					Fe2-O3	1.829(13)			Fe3-Fe3	2.796(25)	x2
									Fe3-Fe3	2.63839(31)	x2
									Fe3-O1	1.70(5)	x2
									Fe3-O1	1.97(6)	
									Fe3-O2	1.768(22)	x2
									Fe3-O3	1.64(8)	

Table 2. Volume and unit-cell parameters for h-Fe_3O_4 and for the new high pressure phase with pressure obtained with gold unit-cell parameter.

P (GPa)	V (Å^3)	a (Å)	b (Å)	c (Å)	a (Å) Gold
11.0(1)	260.7(4)	9.512(17)	9.635(11)	2.845(4)	4.003(0)
18.4(2)	254.4(3)	9.405(11)	9.529(8)	2.839(3)	3.964(1)
25.7(9)	245.9(2)	9.364(8)	9.421(5)	2.787(2)	3.929(4)
26.3(9)	245.9(2)	9.355(8)	9.421(5)	2.790(2)	3.927(4)
44.7(6)	231.1(1)	9.248(3)	9.231(2)	2.707(1)	3.859(2)
44.8(4)	231.1(1)	9.246(3)	9.234(2)	2.707(1)	3.859(1)
53.9(4)	222.4(1)	9.095(4)	9.147(2)	2.674(1)	3.831(1)
51.6(1.3)	222.3(1)	9.063(3)	9.161(2)	2.678(1)	3.838(4)
53.1(5)	222.3(5)	9.054(3)	9.168(2)	2.678(1)	3.833(2)
64.2(1)	213.4(1)	8.908(4)	9.075(3)	2.639(1)	3.803(0)
64.4(1)	213.4(1)	8.909(4)	9.075(3)	2.639(1)	3.802(0)
64.3 [(a)]	212.3(0)	8.881(2)	9.055(1)	2.640(0)	3.084(1) [(a)]
73.2(1.1)	613.2(5)	8.841(6)	7.933(6)	8.743(7)	3.780(3)
76.4 [(a)]	600.7(9)	8.851(1)	7.837(1)	8.660(1)	3.038(1) [(a)]
87.2(6)	592.7(4)	8.742(6)	7.873(6)	8.612(7)	3.749(1)
88.5(2)	586.6(6)	8.671(9)	7.822(11)	8.649(14)	3.746(0)
103.1(2.0)	577.9(8)	8.517(12)	7.771(15)	8.731(18)	3.717(4)

[(a)]data corresponding to the run 3 where pressure value is obtained with Neon.

Table 3. Equation of state parameters for h- Fe_3O_4 compared with the literature.

	V_0 (Å^3)	K_0 (GPa)	K'
This study (up to 64 Gpa)	287 (4)	124 (12)	4
This study (up to 46 Gpa)	277 (2)	172 (8)	4
Haavik et al. (2000)	278.24	202 (7)	4
Dubrovinsky et al. (2003)	277.9 (4)	198 (5)	4
Bengston et al. (2013)	270.7	189	4.02
Ju et al. (2012)	-	234.2 (2.5)	2.70 (09)

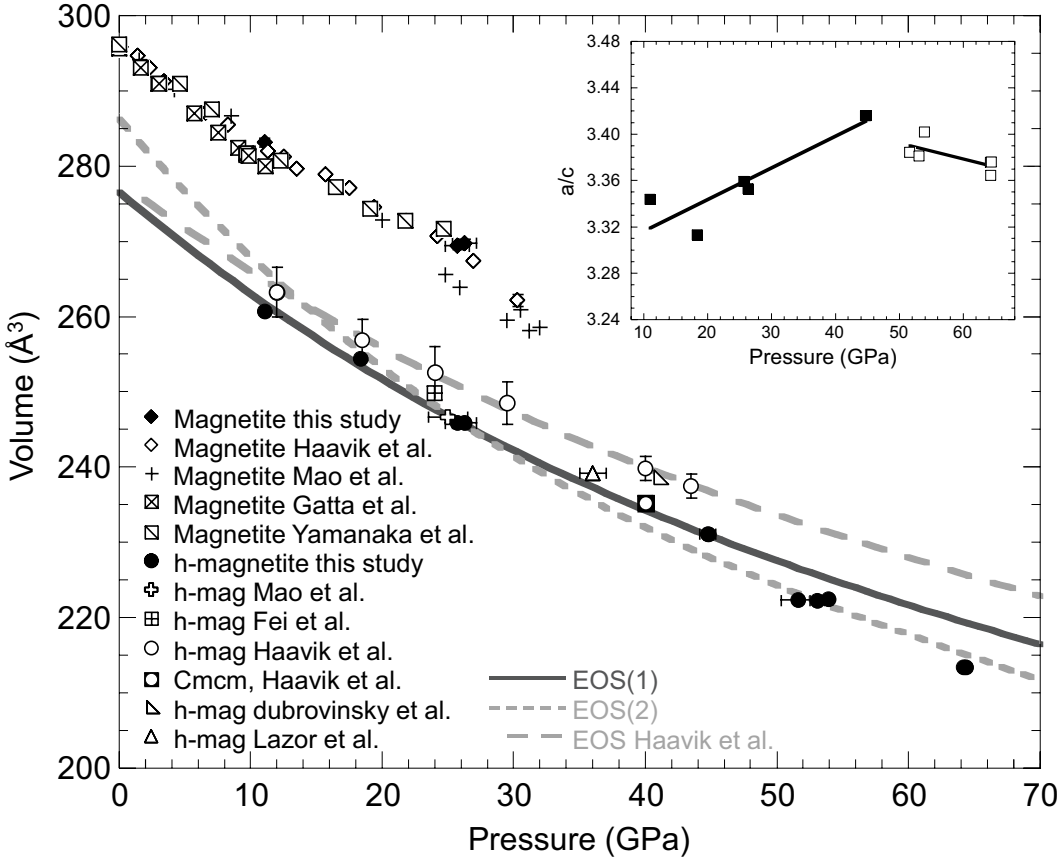
Volume (Å^3)
Pressure (GPa)
Magnetite this study
Magnetite Haavik et al.
Magnetite Mao et al.
Magnetite Gatta et al.
Magnetite Yamanaka et al.
h-magnetite this study
h-mag Mao et al.
h-mag Fei et al.
h-mag Haavik et al.
Cmcm, Haavik et al.
h-mag dubrovinsky et al.
h-mag Lazor et al.
EOS(1)
EOS(2)
EOS Haavik et al.
a/c
Pressure (GPa)

Figure 1

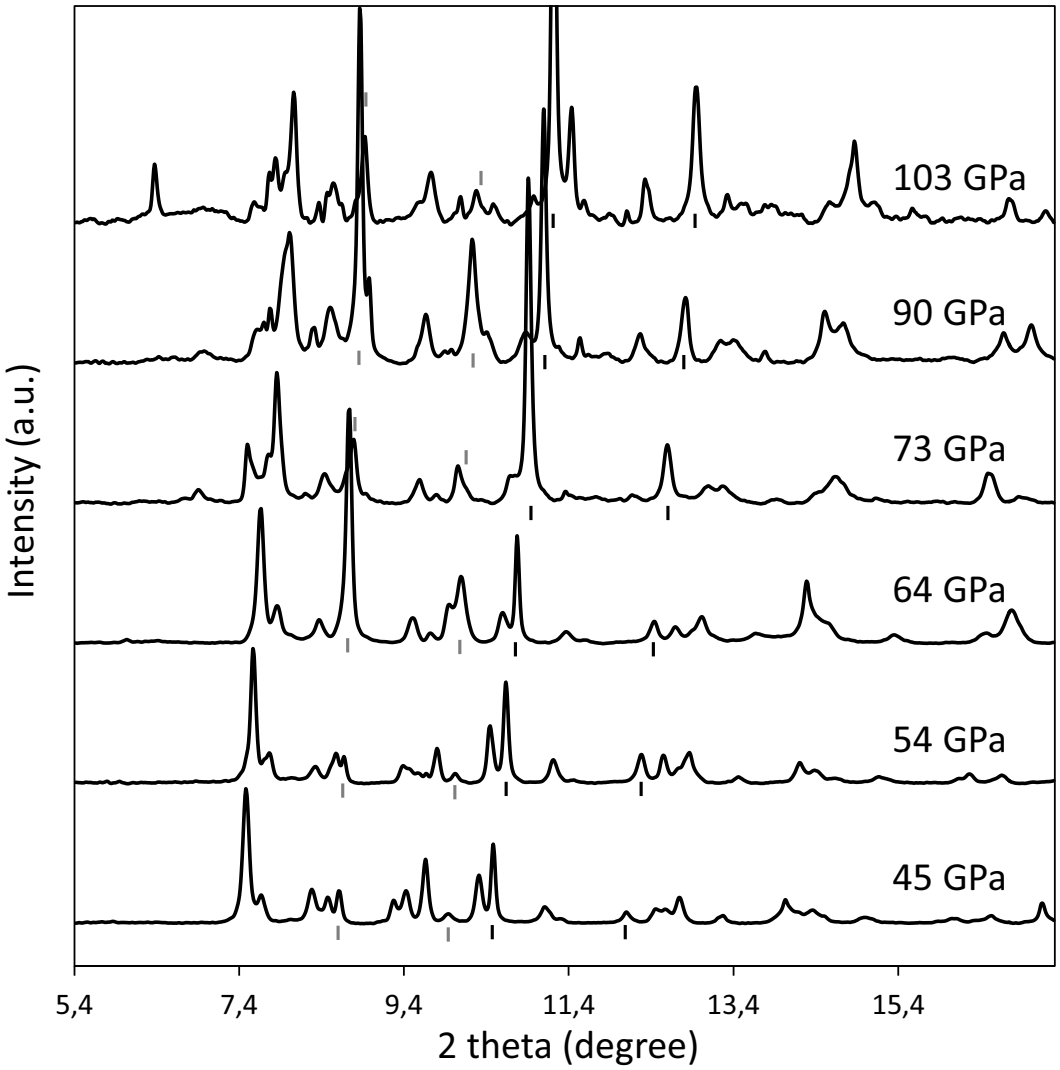
103 GPa
90 GPa
73 GPa
64 GPa
54 GPa
45 GPa
Intensity (a.u.)
5,4
7,4
9,4
11,4
13,4
15,4
2 theta (degree)

Figure 2

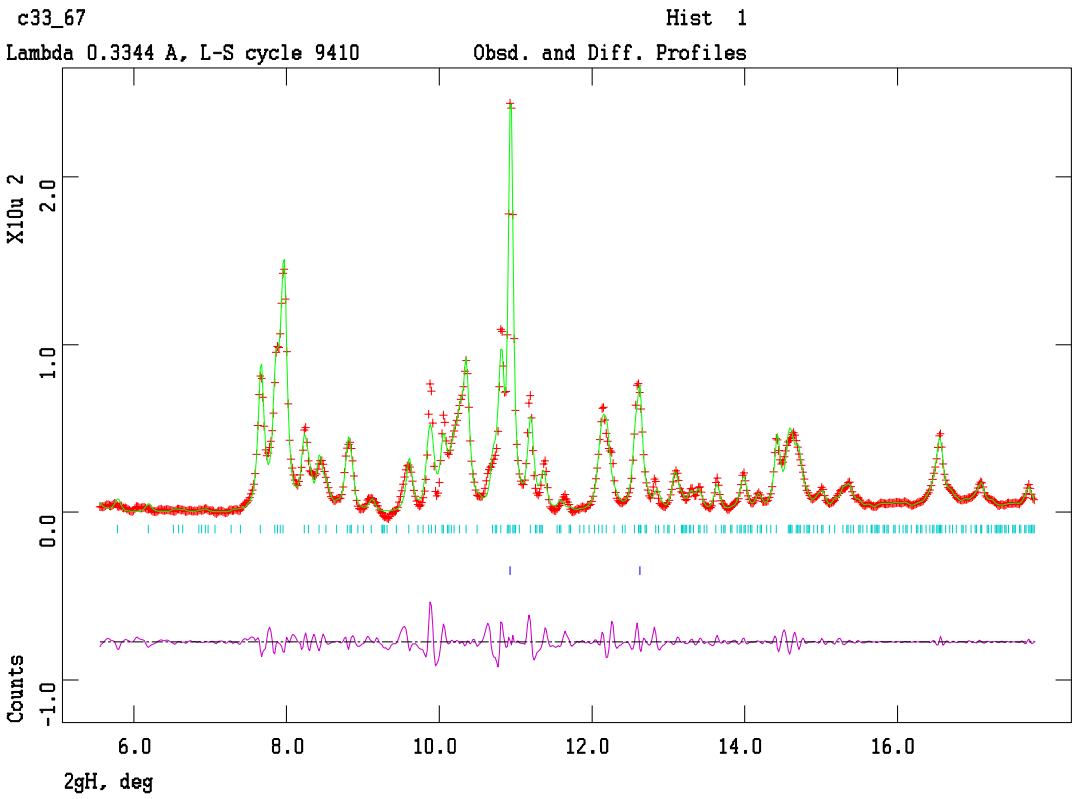
c33_67
Hist 1
Lambda 0.3344 A, L-S cycle 9410
Obsd. and Diff. Profiles
X10u 2
2.0
1.0
0.0
-1.0
Counts
6.0
8.0
10.0
12.0
14.0
16.0
2gH, deg

Figure 3

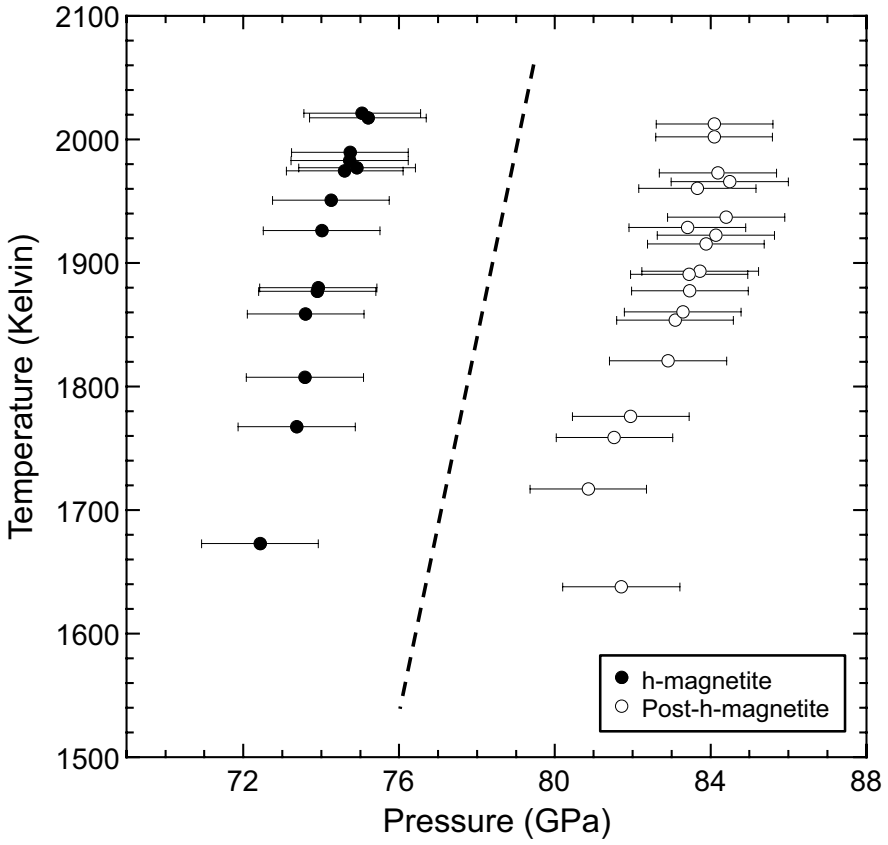
2100
2000
1900
1800
1700
1600
1500
Temperature (Kelvin)
72
76
80
84
88
Pressure (GPa)
h-magnetite
Post-h-magnetite

Figure 4

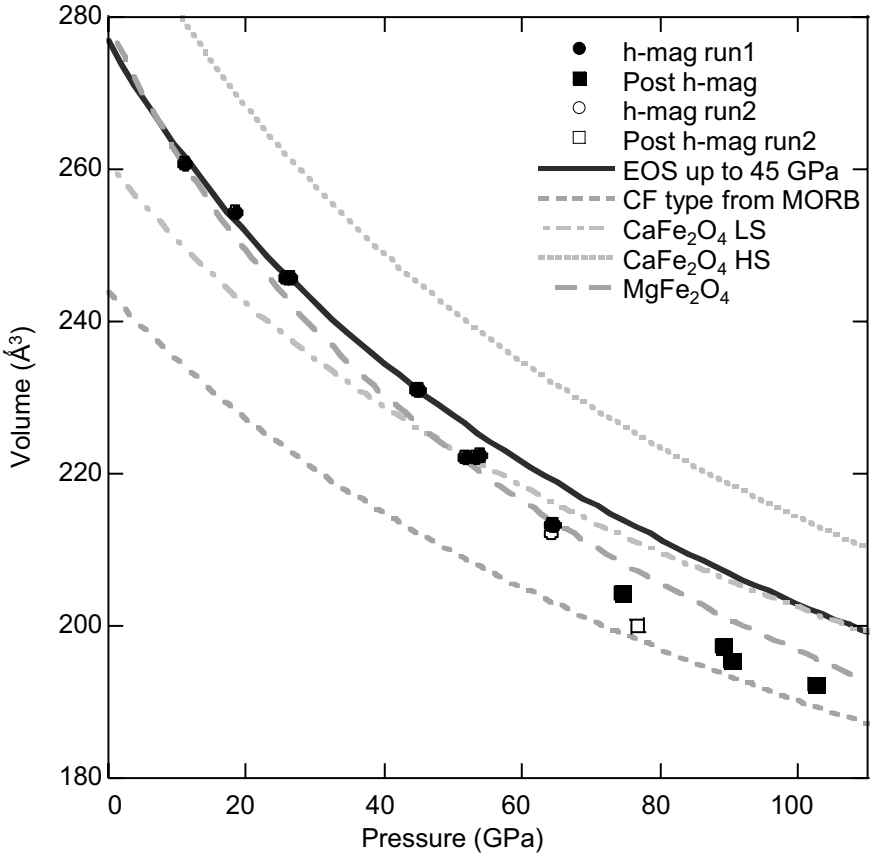
280
260
240
220
200
180
Volume (Å³)
0
20
40
60
80
100
Pressure (GPa)
h-mag run1
Post h-mag
h-mag run2
Post h-mag run2
EOS up to 45 GPa
CF type from MORB
CaFe2O4 LS
CaFe2O4 HS
MgFe2O4

Figure 5